Optical-model description of $^{16}O + ^{28}Si$ elastic scattering at backward angles

K. O. Terenetski* and J. D. Garrett
Niels Bohr Institute, University of Copenhagen, Copenhagen, Denmark
(Received 19 April 1978; revised manuscript received 21 June 1978)

The large, oscillating backward angle cross sections that have been observed in recent $^{16}O + ^{28}Si$ elastic data at $E(^{16}O) = 50$ and 55 MeV are reproduced in an optical-model analysis using Woods-Saxon potentials.

[NUCLEAR REACTIONS ^{28}Si (^{16}O, ^{16}O), $E = 50$ and 55 MeV; calculated $\sigma(\theta)$; deduced optical-model parameters.]

Recent measurements[1-3] of the elastic scattering of ^{16}O and $^{12}C + ^{28}Si$ at backward angles have found unexpected large cross sections that oscillate as a function of angle. Initial attempts to reproduce the details of such data using optical model potentials were unsuccessful.[2] These data, however, have been reproduced by introducing a surface wave resonance into the optical model using a Regge pole,[2,4] in terms of the WKB approximation,[5] using an l-dependent optical potential,[6] and with surface transparent potentials.[7] The present communication reports an optical-model analysis of the $^{16}O + ^{28}Si$ data[2,4] at 50 and 55 MeV incident energy.

The procedure used in the analysis consisted of three steps. (i) The elastic cross section $d\sigma_{el}$ in the angular interval, where $d\sigma_{el}$ is greater than 0.1 times the Rutherford cross section $d\sigma_{Ruth}$, was fitted[8] with several different optical potentials. From the intersection of these potentials, it was determined that the elastic scattering fixes[9] the real nuclear potential U_N to be -0.75 MeV at a separation of 9.02 fm for the 50 MeV data and -0.8 MeV at a separation of 8.92 fm for the 55 MeV data. (ii) Next, the real part of the nuclear potential was obtained by fitting the elastic data in the angular interval where $d\sigma_{el} \gtrsim 10^{-3}\, d\sigma_{Ruth}$. Four parameter Woods-Saxon potentials with identical real and imaginary geometry were used in this part of the analysis. The strength of the real potential V, the radius parameter r_0, and the diffusivity a were varied while requiring that $U_N(9.02) = -0.75$ MeV and $U_N(8.92) = -0.8$ MeV for 50 and 55 MeV, respectively. The imaginary potential strength was fixed at 20% of the real potential strength during these calculations to obtain the real potential. It was observed that the rate of the decrease of the elastic cross section from $d\sigma_{Ruth}$ was particularly sensitive to the diffusivity a, and that the oscillations, which appear for $d\sigma_{el} < 0.1\, d\sigma_{Ruth}$, are sensitive to V and r_0. (iii) Finally, the imaginary potential strength W and the imaginary radius parameter r_i were varied to obtain the best fit for $\theta_{c.m.} \gtrsim 140°$. The angular spacing of the back angle oscillations is not particularly sensitive to the variations in the imaginary potential, but the overall back angle cross sections and the amplitude of the oscillations are very sensitive to the details of the imaginary potential.

The resulting predicted cross sections are shown as solid curves with the experimental data[2,4] in Fig. 1. In the case of the 50 MeV data, the details of the cross section forward of 90° and backward of 120° are reproduced very well. Even the angular region $135 \lesssim \theta_{c.m.} \lesssim 150°$, where oscillations are not observed in the experimental cross sections, is reproduced qualitatively. Between 90 and 120°, however, four maxima are observed in the data and only three are predicted. The features of the 55 MeV elastic angular distribution also are reproduced using the fitting procedure described above (see the full drawn curve in Fig. 1). It is difficult, however, to reproduce the onset of the oscillations in $\sigma_{el}(50 \lesssim \theta_{c.m.} \lesssim 70)$, while requiring that $U_N(8.92) = -0.8$ MeV. A second calculation, in which $U_N(8.92)$ is decreased to -1.3 MeV, is shown (dashed curve) with the 55 MeV data. Both the onset of the oscillations in σ_{el} and the positions of the maxima for the backward angle cross sections are better reproduced by the dashed curve. The forward angle elastic cross sections ($\theta_{c.m.} \lesssim 50°$), however, are not reproduced when the real nuclear potential is allowed to vary from -0.8 MeV at an ion-ion separation of 8.92 fm (i.e., by the dashed curve in Fig. 1).

The optical model parameters used in the calculations are contained in Table I. Identical real geometry was used for the set I potentials that were obtained using the three step prescription described above. Between the two incident energies the strength of the real potential V for parameter sets I was changed so that at 50 MeV, $U_N(9.02) = -0.75$ MeV and at 55 MeV, $U_N(8.92) = -0.8$ MeV. These are the values of the real nuclear potential determined from the intersection of several potentials, which fit forward angle cross sections

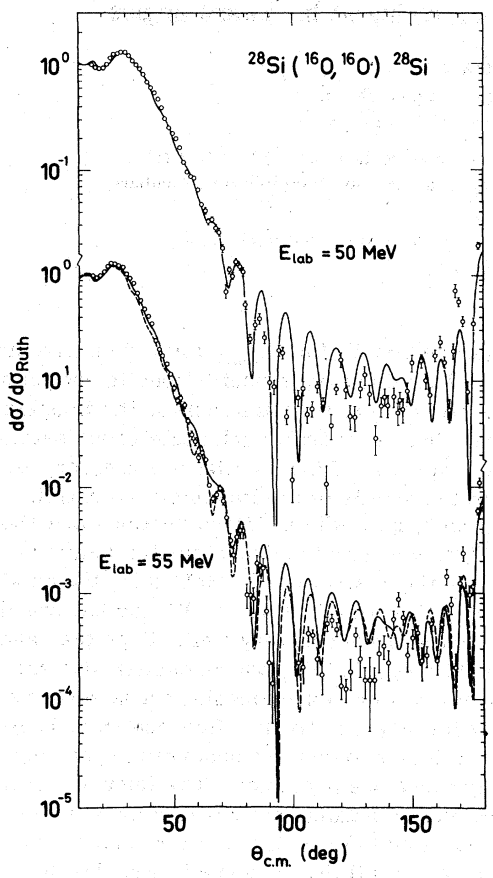

FIG. 1. Comparison of $^{16}O+^{28}Si$ elastic data with optical model predictions. The elastic data are from Refs. 2 and 4. The optical-model analysis is described in the text, and the resulting parameters are given in Table I. For the 55 MeV data the solid and dashed curves correspond to optical-model parameter sets I and II, respectively.

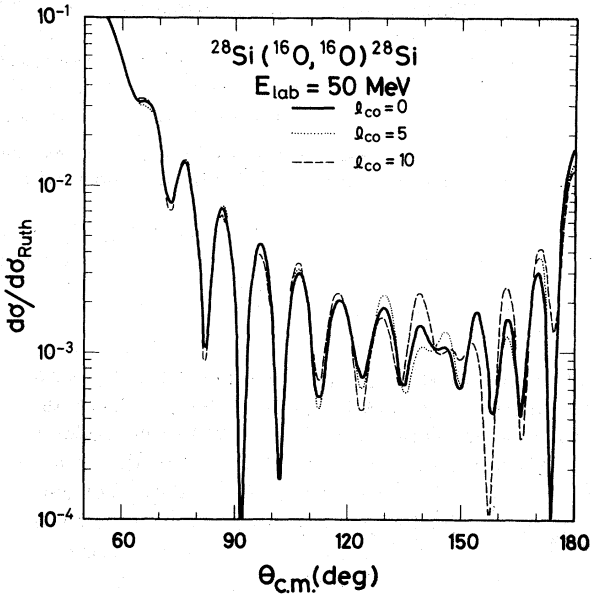

FIG. 2. Comparison of the optical-model prediction shown with the 50 MeV data in Fig. 1 with calculations based on the same potentials with the lowest 5 ($l_{co}=5$) and the lowest 10 ($l_{co}=10$) partial waves removed. For this calculation the transmission coefficients drop to 0.5 between $l=22$ and 23.

(see above). The small adjustment of r_i was necessary to reproduce the magnitude of the cross sections and the amplitude of the oscillations at backward angles. The resulting increase in the imaginary potential in the surface region at the higher incident energy would be expected because additional exit channels are available. All the potentials obtained are characterized by weak absorption. Calculations with the lower partial waves removed (see Fig. 2) indicate that, even though contributions from "interior" partial waves do affect the details of the back angle data, the basic character of the backward angle cross section does not depend on the lowest partial waves.

These potentials are very different from the strongly absorbing "unique energy-independent" potentials,[10] which have been obtained from fitting forward angle $^{16}O+^{28}Si$ elastic data as a function of incident energy. The unique energy-independent potentials do not reproduce the backward angle

TABLE I. Optical-model parameters.

$E_{inc}(^{16}O)$ (MeV)	V (MeV)	r_0 (fm)	a (fm)	W (MeV)	r_i (fm)	a_i (fm)	r_C[a] (fm)
50 Set I	−160.00	1.152	0.49	−10.0	1.1199	0.49	1.3
55 Set I	−137.48	1.152	0.49	−10.0	1.1750	0.49	1.3
Set II	−160.00	1.1816	0.49	−10.0	1.2322	0.49	1.3

$$U_N(r)=V\left[1+\exp\left(\frac{r-R}{a}\right)\right]^{-1}+iW\left[1+\exp\left(\frac{r-R_i}{a_i}\right)\right]^{-1},$$

where $R=r_0(16^{1/3}+28^{1/3})$ and $R_i(16^{1/3}+28^{1/3})$.

[a] Radius of Coulomb potential given by $R_C=r_C(16^{1/3}+28^{1/3})$.

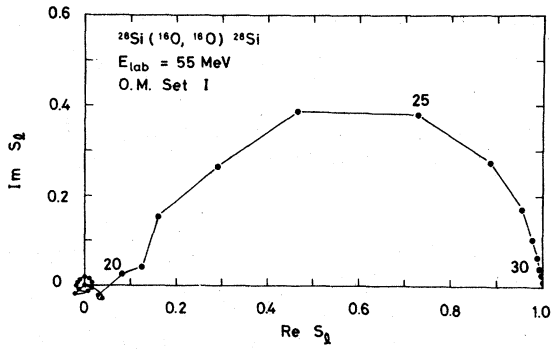

FIG. 3. Argand diagram for the S-matrix elements corresponding to potential set I for the $^{16}O+ ^{28}Si$ elastic scattering at $E(^{16}O)= 55$ MeV. The matrix elements corresponding to $l= 20$, 25, and $30\hbar$ are indicated on the figure. The optical-model parameters are given in Table I, and the predicted cross sections are shown as solid lines with the experimental data in Fig. 1.

data.[2] Conversely, without the addition of energy-dependent terms, the potentials proposed in this work would not be expected to reproduce $^{16}O+^{28}Si$ elastic scattering at higher incident energies.

The present analysis describes the cross sections in the angular range $90 \lesssim \theta_{c.m.} \lesssim 140°$ better than the recently reported[6] analysis based on l-dependent optical-model potentials. The S matrices generated by the potentials from the present analysis (see Fig. 3) are considerably different from those derived from either the Regge-pole[2,4] or l-dependent optical-model[6] analyses (compare with Fig. 2 of Ref. 6), even though all these calculations qualitatively reproduce the cross sections at backward angles.

In summary, a prescription is presented for an optical-model analysis of the large backward angle cross sections observed[1-4] in recent ^{12}C and ^{16}O elastic scattering measurements on ^{28}Si. This prescription is applied to existing $^{16}O+^{28}Si$ elastic data[2,4] at 50 and 55 MeV incident energy. The Woods-Saxon potentials obtained reproduce most of the features of the $^{16}O+^{28}Si$ elastic scattering angular distributions at these two bombarding energies. It will be interesting to ascertain whether the more detailed elastic and inelastic $^{16}O+^{28}Si$ data which presently are being obtained,[1] can be explained in terms of the optical model.

We wish to acknowledge discussions with Professor Aa. Winther and to thank Dr. P. Braun-Munzinger for furnishing us with the 50 MeV $^{16}O+^{28}Si$ elastic data prior to its publication. This work was supported by the Danish Natural Science Research Council and the Commemorative Association of the Japan World Exposition.

---

*Permanent affiliation: Institute for Nuclear Research, Ukrainian Academy of Science, Prospect Nauki 119, Kiev-28, 252028, USSR.

[1]Proceedings of Symposium on Heavy Ion Elastic Scattering, Rochester, 1977, edited by R. M. de Vries (unpublished).

[2]P. Braun-Munzinger, G. M. Berkowitz, T. M. Cormier, C. M. Jachcinski, J. W. Harris, J. Barrette, and M. J. LeVine, Phys Rev. Lett. 38, 944 (1977).

[3]M. R. Clover, R. M. DeVries, R. Ost, N. Rust, R. N. Cherry, Jr., and H. E. Gove, in Proceedings of the International Conference on Nuclear Structure: Contributed papers (International Academic, Tokyo, 1977), p. 606.

[4]P. Braun-Munzinger and J. Barrette, Ref. 1, p. 85.

[5]S. Landowne and Aa. Winther, Ref. 1, p. 525; and private communication.

[6]V. Shkolnik, D. Dehnhard, L. Kubono, M. A. Franey, and S. Tripp, Phys. Lett. 74B, 195 (1978); and D. Dehnhard, Ref. 1, p. 20.

[7]E. H. Auerbach, A. J. Baltz, M. Golin, and S. H. Kahana in Ref. 1, p. 394.

[8]A heavy-ion version of the optical model search code GENOA of F. G. Perey, L. W. Owen, S. D. Blazier, and C. Y. Wong (unpublished) was used for all elastic calculations.

[9]It is well known that the elastic scattering determines the real ion-ion potential at a particular separation distance. See, e.g., G. R. Satchler, in *Proceedings of the International Conference on Reactions between Complex Nuclei, Nashville, 1974*, edited by R. L. Robinson *et al.* (North-Holland, Amsterdam, 1974), Vol. II, p. 171; and F. Videbaek, R. B. Goldstein, L. Grodzins, S. G. Steadman, T. Belote, and J. D. Garrett, Phys. Rev. C 15, 954 (1977).

[10]J. G. Cramer, R. M. DeVries, D. A. Goldberg, M. A. Zisman, and C. F. Maguire, Phys. Rev. C 14, 2158 (1976).